Cell Reports

USP7 protects TFEB from proteasome-mediated degradation

Graphical abstract

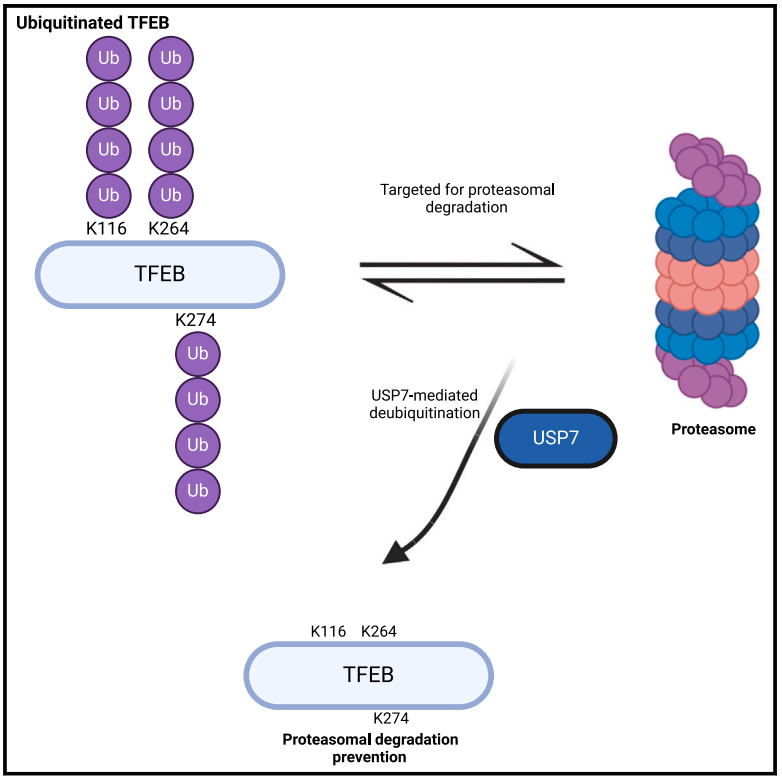

Highlights

- The deubiquitinase USP7 interacts with TFEB
- USP7 removes ubiquitin from TFEB at K116, K264, and K274
- USP7 protects TFEB from proteasome-mediated degradation
- USP7 preserves TFEB-mediated transcriptional responses and positively regulates autophagy

Authors

Swati Keshri, Mariella Vicinanza, Michael Takla, David C. Rubinsztein

Correspondence

dcr1000@cam.ac.uk

In brief

Keshri et al. identify USP7 as a deubiquitinase for TFEB, a master transcriptional regulator of lysosome biogenesis and autophagy. USP7 removes ubiquitin from TFEB and protects it from proteasomal degradation, thereby preserving TFEB-mediated transcriptional responses to starvation and acting as a positive regulator of autophagy.

Keshri et al., 2024, Cell Reports *43*, 114872
November 26, 2024
https://doi.org/10.1016/j.celrep.2024.114872

CellPress

Cell Reports

CellPress
OPEN ACCESS

Report

USP7 protects TFEB from proteasome-mediated degradation

Swati Keshri,[1,2] Mariella Vicinanza,[1,2] Michael Takla,[1,2] and David C. Rubinsztein[1,2,3,*]
[1]Cambridge Institute for Medical Research, University of Cambridge, CB2 0XY Cambridge, UK
[2]UK Dementia Research Institute, Cambridge Biomedical Campus, Cambridge, UK
[3]Lead contact
*Correspondence: dcr1000@cam.ac.uk
https://doi.org/10.1016/j.celrep.2024.114872

SUMMARY

The transcription factor EB (TFEB) is a master regulator of lysosomal biogenesis and autophagy. We identify a distinct nuclear interactome of TFEB, with ubiquitin-specific protease 7 (USP7) emerging as a key post-translational modulator of TFEB. Genetic depletion and inhibition of USP7 reveal its critical role in preserving TFEB stability within both nuclear and cytoplasmic compartments. Specifically, USP7 is identified as the deubiquitinase responsible for removing the K48-linked polyubiquitination signal from TFEB at lysine residues K116, K264, and K274, thereby preventing its proteasomal degradation. Functional assays demonstrate the involvement of USP7 in preserving TFEB-mediated transcriptional responses to nutrient deprivation while also modulating autophagy flux and lysosome biogenesis. As USP7 is a deubiquitinase that protects TFEB from proteasomal degradation, these findings provide the foundation for therapeutic targeting of the USP7-TFEB axis in conditions characterized by TFEB dysregulation and metabolic abnormalities, particularly in certain cancers.

INTRODUCTION

Transcription factor EB (TEFB) is a member of the microphthalmia transcription factor (MiT/TFE) family, which also includes other members, such as microphthalmia-associated transcription factor (MITF), TFE3, and TFEC in mammals. MiT/TFE transcription factors share a conserved basic-helix-loop-helix (bHLH) domain and a leucine zipper (Zip) region.[1,2] The bHLH domain facilitates DNA binding, while the Zip region is crucial for dimerization, enabling the formation of homo- and heterodimers with other family members.[2] TFEB plays a vital role in cellular adaptation to various stresses, including nutrient deprivation, oxidative and endoplasmic reticulum stress, and DNA and mitochondrial damage, and is a master regulator of autophagy and lysosomal biogenesis.[3–9]

Post-translational modifications (PTMs) determine the localization and activity of TFEB, regulating its function. TFEB is inactive when cytosolic but can regulate transcription when translocated to the nucleus.[4] Phosphorylation is a vital PTM for this process and is regulated by kinases, such as the mammalian target of rapamycin complex 1 (mTORC1), a serine/threonine kinase. mTORC1 acts as a central signaling hub that responds to stress and integrates various environmental cues to regulate TFEB.[10] It phosphorylates TFEB at specific sites, including S122, S142, and S211, when amino acids are abundant. In contrast, under amino acid-deficient conditions, mTORC1 activity is inhibited.[11–15] The inhibition allows TFEB to translocate to the nucleus, which is crucial for activating gene expression programs that aid cellular adaptation and survival in nutrient-deprived environments. Other PTMs include, but are not limited to, acetylation, SUMOylation, and ubiquitination.[16–18]

TFEB dysregulation is associated with various pathological conditions, such as neurodegenerative diseases, lysosomal storage disorders, metabolic disorders, and cancer.[19–24] Therefore, it is crucial to investigate additional mechanisms that fine-tune TFEB activity.

This study examines the TFEB protein interaction network in response to nutrient deprivation using mass spectrometry (MS) analysis to identify factors that may affect TFEB signaling. We identified a set of nuclear interacting proteins for TFEB to which we refer as the "nuclear TFEB interactome." Among these candidates, we focused on ubiquitin-specific protease 7 (USP7), a 130-kDa multidomain deubiquitinating enzyme belonging to the USP family.[25] It is involved in various cellular pathways, such as the DNA damage response, transcriptional regulation, cell cycle progression, and apoptosis.[26–28] USP7 is predominantly nuclear and consists of three subdomains: a tumor necrosis factor-associated factor (TRAF)-like domain responsible for substrate recognition, a central catalytic core that contributes to enzymatic activity, and a herpes virus-associated ubiquitin-like (HUBL) domain containing five Ubl domains.[29–31] The subcellular localization of USP7 is primarily facilitated by its N-terminal domain, largely through interactions with several nuclear proteins, including p53, MDM2, TRAF4, and TRAF1.[29] It has been postulated that these interactions may facilitate nuclear translocation, particularly in pathways associated with DNA damage repair and transcriptional regulation. Despite

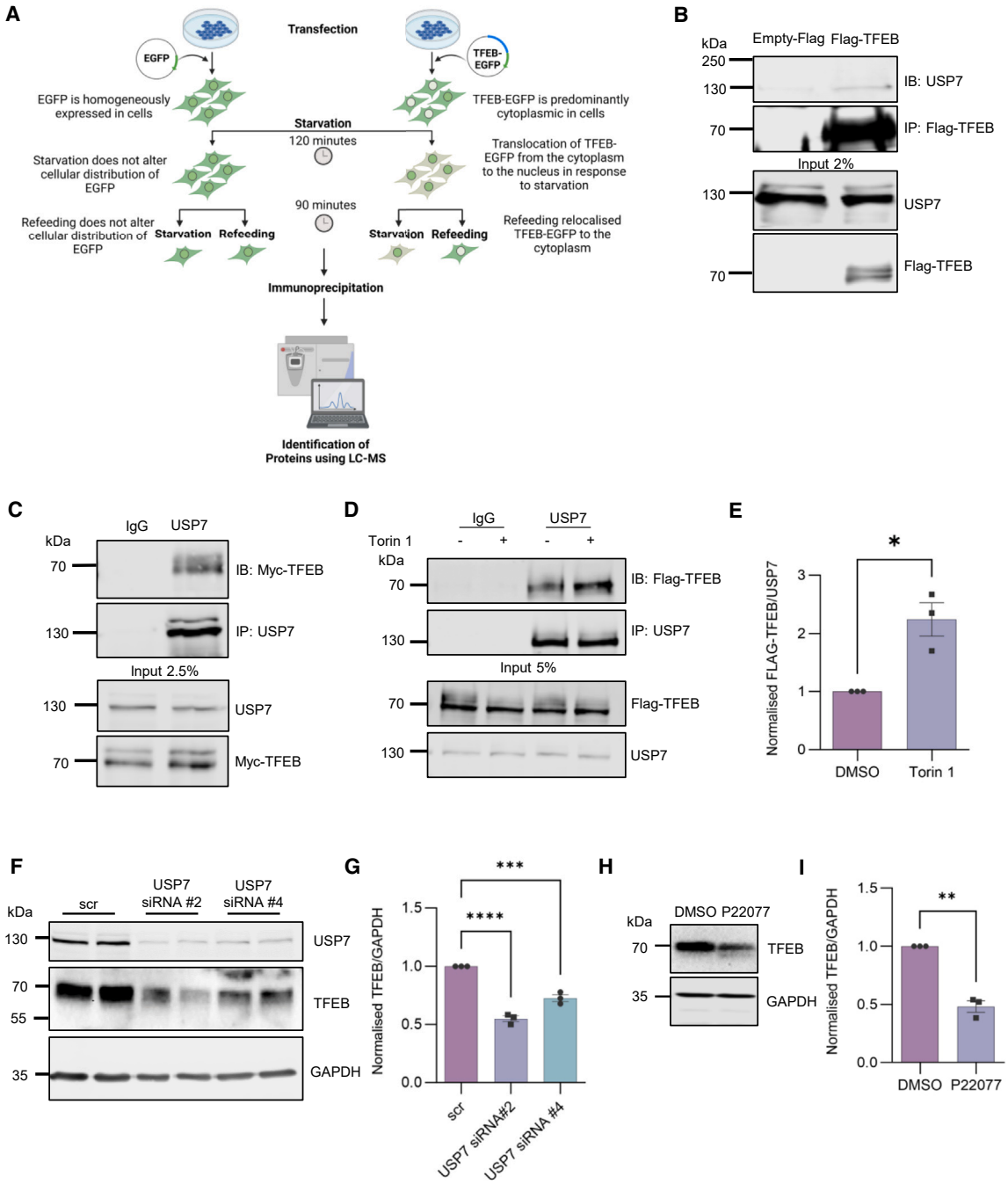

Figure 1. USP7 regulates TFEB protein stability as a component of the starvation-induced TFEB nuclear interactome

(A) Schematic of the experimental approach used to identify TFEB-EGFP-interacting proteins under amino acid starvation conditions via liquid chromatography-mass spectrometry (LC-MS). Created with BioRender.

(B) HeLa cells were transfected with FLAG-TFEB for 24 h, followed by amino acid starvation for 2 h, before harvesting for IP. Western blot analysis demonstrates the coIP of endogenous USP7 with FLAG-TFEB. $n = 3$.

(C) Reverse coIP experiment. HeLa cells overexpressed Myc-TFEB for 24 h, followed by 2 h of amino acid starvation. Endogenous USP7 pull-down showed coIP with Myc-TFEB. $n = 3$.

(D and E) TFEB KO HeLa cells were transfected with FLAG-TFEB overnight. The next day, cells were treated with 1 μM Torin 1 for 2 h, followed by IP of endogenous USP7. Representative western blot shows increased TFEB co-immunoprecipitated with USP7 following Torin 1 treatment. Data are presented as normalized mean ± SEM, $n = 3$. Paired two-tailed Student's t test, $^*p < 0.05$ (DMSO vs. Torin 1).

(F and G) HeLa cells were transfected with 50 nM of two distinct siRNAs (#2 and #4) targeting USP7 for 48 h. Western blot analysis indicates a significant reduction in TFEB protein levels upon USP7 knockdown (KD) compared to scrambled control, as shown in the representative blot. Quantification is shown in (G). Data are

(legend continued on next page)

having a range of nuclear substrates, USP7 has also been observed to deubiquitinate cytosolic substrates; for instance, Axin, a key component of the Wnt signaling pathway.[32] The catalytic domain contains the catalytic triad, which coordinates the cleavage of ubiquitin from substrates and is composed of the conserved residues C223, H464, and D481.[30] The oncogenic potential of USP7 is substantial, primarily due to its role in modulating MDM2 stability, which directly influences the levels of the tumor suppressor p53.[33] This regulation plays a pivotal role in the attenuation of p53-mediated apoptotic pathways, thereby promoting tumor formation. Consequently, USP7 represents a promising therapeutic target in cancer, where further investigation of its downstream substrates, including previously uncharacterized ones, could provide deeper insights into its oncogenic mechanisms.

Substrates targeted for proteasomal degradation are marked with a ubiquitin signal through a three-step process involving E1, E2, and E3 enzymes.[34,35] In 2017, Sha et al. discovered that the E3 ubiquitin ligase STUB1 interacts with phosphorylated TFEB, leading to the ubiquitination and preferential degradation of transcriptionally inactive TFEB.[18] However, the precise mechanisms regulating TFEB turnover within the nucleus remain unclear. The presence of the nuclear proteasome and the localization of E3 ligases such as STUB1 and HERC2, which are crucial in regulating the TFEB turnover, in both the cytosol and the nucleus suggests that TFEB degradation may occur not solely in the cytosol but also within the nucleus.[36–38] This paper explores the mechanisms governing TFEB turnover with a particular focus on the potential role of USP7, identified as an interacting protein through mass spectrometry (MS), in preventing TFEB protein degradation.

RESULTS

USP7, a component of the starvation-induced TFEB nuclear interactome, regulates TFEB protein stability

In order to identify nuclear TFEB interactors, we used the affinity purification (AP)-based MS approach outlined in Figure 1A. Initial sensitization of TFEB-EGFP- or EGFP-overexpressing cells to amino acid starvation triggered nuclear translocation of TFEB, while EGFP localization remained unaffected. We subjected the cells to two different treatments. First, we induced prolonged starvation to promote nuclear accumulation of TFEB. Second, we enabled the translocation of TFEB into the cytoplasm by re-feeding the cells with medium supplemented with amino acids.

By exploiting these different cellular states, we identified two complementary sets of TFEB-binding proteins: cytosolic interactors from the refeeding condition and nuclear interactors from the starvation condition. In addition to confirming the presence of known TFEB interactors, such as other MITF family transcription factors, mTOR, XPO1, and 14-3-3 protein (particularly in the TFEB-EGFP condition and not in the EGFP-only control), we also identified a selection of distinctive protein hits. This comprehensive analysis revealed a distinct set of nuclear interaction partners for TFEB, termed the nuclear TFEB interactome (Table S1).

We selected USP7 for further investigation of TFEB regulation, as it is a deubiquitinating enzyme that we hypothesized may play a role in TFEB turnover or activity modulation. We confirmed the interaction between USP7 and TFEB using co-immunoprecipitation (coIP) experiments conducted under the same conditions as the AP-MS analysis (Figure S1A) (Figure 1B). A reverse coIP experiment demonstrated successful coIP of Myc-TFEB when endogenous USP7 was pulled down (Figure 1C). Validation of these interactions was further obtained through a proximity ligation assay. The assay exclusively detected the interaction between the two proteins when antibodies against both proteins were used, confirming their co-localization (Figure S1B). These results support the interaction between USP7 and TFEB in cells, which is consistent with the initial MS findings. Treatment with Torin 1, a compound that inhibits mTORC1-dependent phosphorylation of TFEB and promotes nuclear translocation of TFEB, increased the binding of endogenous USP7 to TFEB (Figures 1D and 1E).

To investigate the effect of USP7 on TFEB turnover, we genetically depleted USP7 using two different oligonucleotides that targeted its coding region. This resulted in a significant decrease in endogenous TFEB protein levels compared to scrambled controls, indicating destabilization of TFEB (Figures 1F and 1G). However, the levels of TFE3, another member of the MiT/TFE family of transcription factors, were not affected by USP7 depletion (Figure S1C). Furthermore, the catalytic function of USP7 appears to be relevant for TFEB stability, as endogenous TFEB protein levels were lowered by the irreversible USP7 inhibitor P22077 (Figures 1H and 1I). Additional USP7 inhibitors (P005091, HBX41108, and XL177A) caused similar reductions in TFEB levels (Figures S1D, S1E, and S2A). These findings confirm that USP7 activity regulates TFEB protein levels. To elucidate the role of STUB1 in the regulation of TFEB and its interaction with USP7, we conducted a series of knockdown (KD) experiments targeting USP7, STUB1, and both proteins simultaneously. Consistent with prior observations, KD of USP7 led to a reduction in endogenous TFEB levels (Figure S2B). However, when both USP7 and STUB1 were knocked down simultaneously, TFEB levels were restored (Figure S2B). This restoration is likely attributable to a decrease in TFEB ubiquitination in the absence of STUB1.

Stabilization of TFEB by USP7 is post-translational and proteasome dependent, protecting TFEB in both the nucleus and cytoplasm

To determine whether the observed decrease in TFEB protein levels upon USP7 loss was post-translational, we used

presented as normalized mean ± SEM, $n = 3$. Ordinary one-way ANOVA with Dunnett's multiple-comparisons post-test, adjusted p value; ****$p < 0.0001$ (scr vs. USP7 siRNA#2), ***$p = 0.002$ (scr vs. USP7 siRNA#4).

(H and I) HeLa cells were treated with 10 μM USP7 inhibitor P22077 for 6 h. Western blot analysis reveals a 50% reduction in endogenous TFEB protein levels following USP7 inhibition compared to DMSO control. Quantification is shown in (I). Data are presented as normalized mean ± SEM, $n = 3$. Paired two-tailed Student's t test, **$p = 0.009$ (DMSO vs. P22077).

IB, immunoblot; IP, immunoprecipitation. See also Figures S1 and S2.

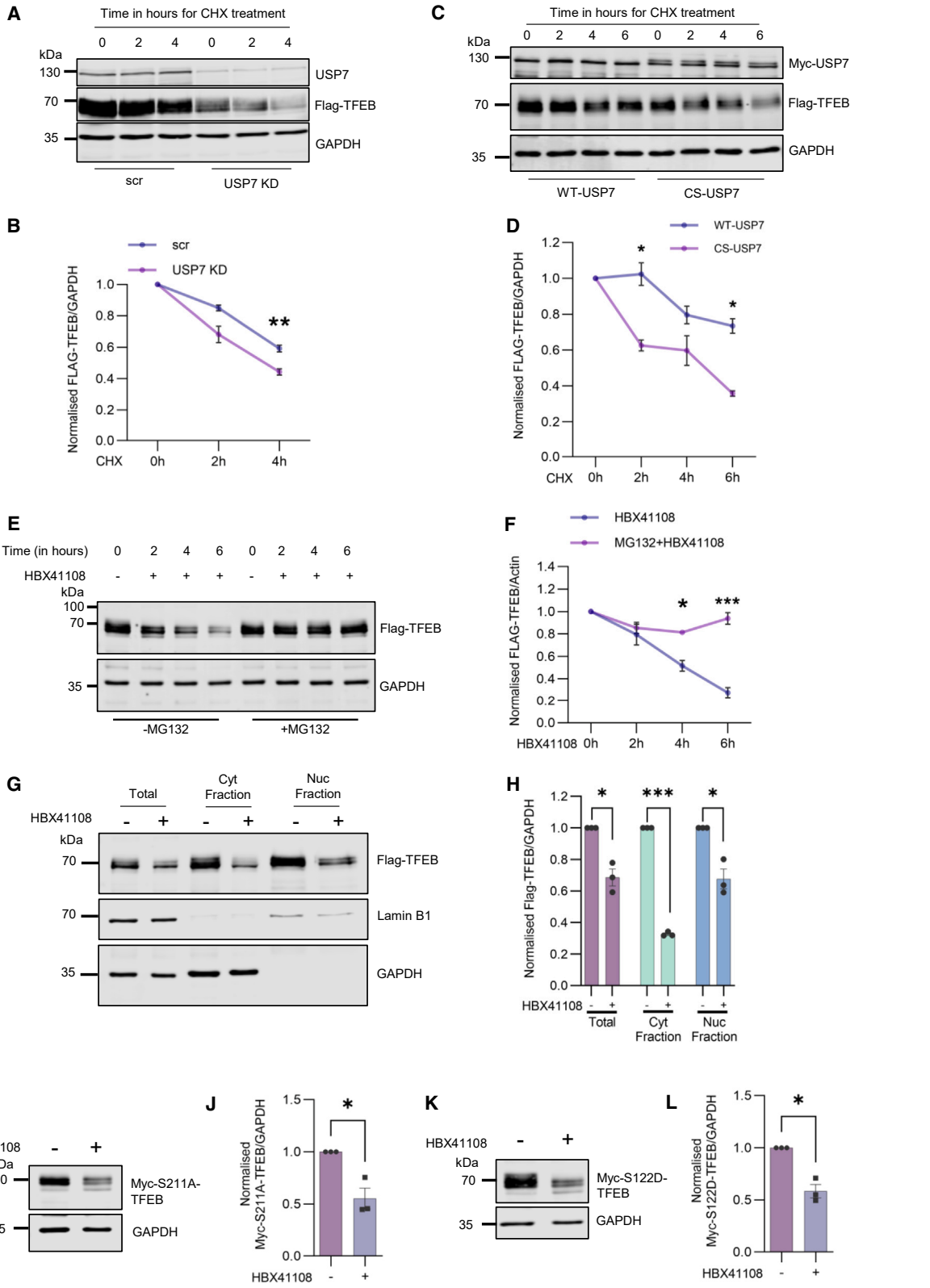

(legend on next page)

cycloheximide (CHX), a translation inhibitor. In the presence of CHX, genetic depletion of USP7 resulted in accelerated degradation of FLAG-TFEB compared to control conditions (Figures 2A and 2B) and of endogenous TFEB upon inhibition of USP7 (Figures S3A and S3B). To investigate whether the catalytic activity of USP7 is essential for its stabilizing effect on TFEB, we reconstituted *USP7* knockout (KO) cells with either wild-type (WT) USP7 or a catalytically dead mutant (C223S [CS]).[39] The WT-USP7 was observed to significantly slow the degradation of FLAG-TFEB, whereas the catalytically inactive CS-USP7 was unable to elicit this effect. This observation corroborates the hypothesis that the catalytic activity of USP7 is crucial for preventing TFEB degradation (Figures 2C and 2D).

To investigate whether the stabilizing effect of USP7 on TFEB is related to the prevention of its proteasomal degradation, we used the proteasomal inhibitor MG132. HeLa cells expressing FLAG-TFEB were pre-treated with MG132 (or DMSO as a control) to inhibit the proteasome before adding the USP7 inhibitor to the medium. While USP7 inhibition significantly reduced FLAG-TFEB protein levels, MG132 prevented this effect (Figures 2E and 2F), suggesting that USP7 buffers proteasome-dependent TFEB degradation.

To evaluate the impact of USP7 inhibition on TFEB levels across different subcellular compartments, we conducted nucleocytoplasmic fractionation following USP7 inhibition. The results revealed a reduction in FLAG-TFEB levels not only in the total cell lysate (input) but also within both cytoplasmic and nuclear compartments (Figures 2G and 2H). Conversely, USP7 overexpression followed by nucleocytoplasmic fractionation showed an increase in total, nuclear, and cytoplasmic TFEB levels (Figures S3C and S3D).

mTORC1-mediated phosphorylation at S142 regulates the degradation of TFEB. STUB1, an E3 ligase, preferentially interacts with phosphorylated TFEB and directs its proteasomal degradation.[18] Accordingly, we assessed the impact of USP7 loss of function on three TFEB phospho-mutants: S211A-TFEB (predominantly nuclear), S122D-TFEB (predominantly cytoplasmic), and S142A-TFEB (known for potentially escaping ubiquitination due to weakened interaction with STUB1) (Figure S3E).[11,14,40] Destabilization of both nuclear (S211A-TFEB) and cytoplasmic (S122D-TFEB) TFEB was observed upon USP7 inhibition (Figures 2I–2L), suggesting that USP7 acts on TFEB in both the nucleus and the cytoplasm. However, the S142A TFEB mutant showed only a slight decrease, which was not statistically significant, suggesting that the reduced ubiquitination of this mutant makes it more stable (because it is not effectively targeted to the proteasome), consistent with previous research.[18] Thus, S142A-TFEB is not obviously dependent on USP7 for its stability (Figure S3F).

These findings collectively demonstrate that USP7 protects TFEB in both the nucleus and cytoplasm from proteasome-dependent degradation.

Subsequently, we investigated the levels of nuclear and cytoplasmic USP7 in response to amino acid starvation conditions using nucleocytoplasmic fractionation. The results revealed a slight increase in cytoplasmic USP7 levels without a significant decrease in nuclear USP7 protein levels (Figures S3G and S3H). Notably, the data also highlight the presence of substantial cytoplasmic USP7, which is consistent with our hypothesis that USP7 plays a role in regulating TFEB even under nutrient-rich conditions. The significant cytoplasmic presence of USP7 supports the idea that, although USP7 is predominantly nuclear, it shuttles between the cytoplasm and nucleus, thereby being capable of regulating cytoplasmic substrates.

In response to amino acid starvation, we observed a slight increase in USP7 protein levels in the cytoplasm (Figures S3G and S3H), which prompted us to investigate USP7 transcript levels. Our analysis revealed a time-dependent increase in USP7 transcript levels in response to amino acid starvation in WT cells but not in HeLa double-KO cells lacking both TFEB and TFE3 (Figure S4A). To further corroborate the dependency of USP7 transcription on these factors, we conducted double-KD

Figure 2. Stabilization of TFEB by USP7 is a post-translational, proteasome-dependent process

Inhibition of USP7 reduces TFEB levels in both cytosolic and nuclear compartments.

(A) HeLa cells were transiently transfected with 50 nM USP7 siRNA (#2) for 48 h to achieve USP7 KD, followed by FLAG-TFEB overexpression for the final 24 h. On day 3, cells were treated with 25 μg/mL CHX at various time points. The representative western blot shows an accelerated degradation of FLAG-TFEB under USP7 KD conditions compared to the scrambled control.

(B) Data are presented as normalized mean ± SEM, $n = 3$. Two-way ANOVA with Bonferroni's multiple-comparisons post-test, adjusted p value; $^{**}p = 0.0066$ (scr vs. USP7 KD, 4 h).

(C) *USP7* KO HEK293 cells were co-transfected with WT-USP7 or catalytically inactive CS-USP7 for 48 h, along with FLAG-TFEB for the final 24 h. On day 3, cells were treated with 25 μg/mL CHX. The representative western blot shows slower degradation of FLAG-TFEB when co-expressed with WT-USP7 compared to CS-USP7.

(D) Data are presented as normalized mean ± SEM, $n = 3$. Two-way ANOVA with Bonferroni's multiple-comparisons post-test, $^{*}p < 0.05$ (WT-USP7 vs. CS-USP7, 2 h and 6 h).

(E and F) HeLa cells overexpressing FLAG-TFEB were treated with the proteasome inhibitor MG132 (10 μM) for 2 h, followed by treatment with the USP7 inhibitor HBX41108 (5 μM) for various times. The representative western blot shows that USP7 inhibition led to a reduction in FLAG-TFEB levels, which was not observed in the presence of the proteasome inhibitor. Quantification is shown in (F). Data are presented as normalized mean ± SEM, $n = 3$. Two-way ANOVA with Šídák's multiple-comparisons post-test, $^{***}p < 0.001$ (HBX41108 vs. MG132+HBX41108, 6 h), $^{*}p < 0.05$ (HBX41108 vs. MG132+HBX41108, 4 h).

(G) HeLa cells overexpressing FLAG-TFEB were treated with the USP7 inhibitor HBX41108 (5 μM) for 6 h before harvesting for nuclear/cytoplasmic fractionation. The representative blot shows a significant reduction in FLAG-TFEB protein levels in both the cytosolic and nuclear fractions following USP7 inhibition.

(H) Data are presented as normalized mean ± SEM, $n = 3$. Paired two-tailed Student's t test, $^{*}p < 0.05$, $^{***}p < 0.001$ (DMSO vs. HBX41108). Cyt, cytoplasmic; Nuc, nuclear.

(I–L) HeLa cells overexpressing Myc-S211A-TFEB (I) and Myc-S122D-TFEB (K) were treated with HBX41108 (5 μM) for 6 h. The western blots in (J) and (L) are representative. Data are presented as normalized mean ± SEM, $n = 3$. Paired two-tailed Student's t test, $^{*}p < 0.05$; ns, not significant (DMSO vs. HBX41108).

See also Figures S3–S8.

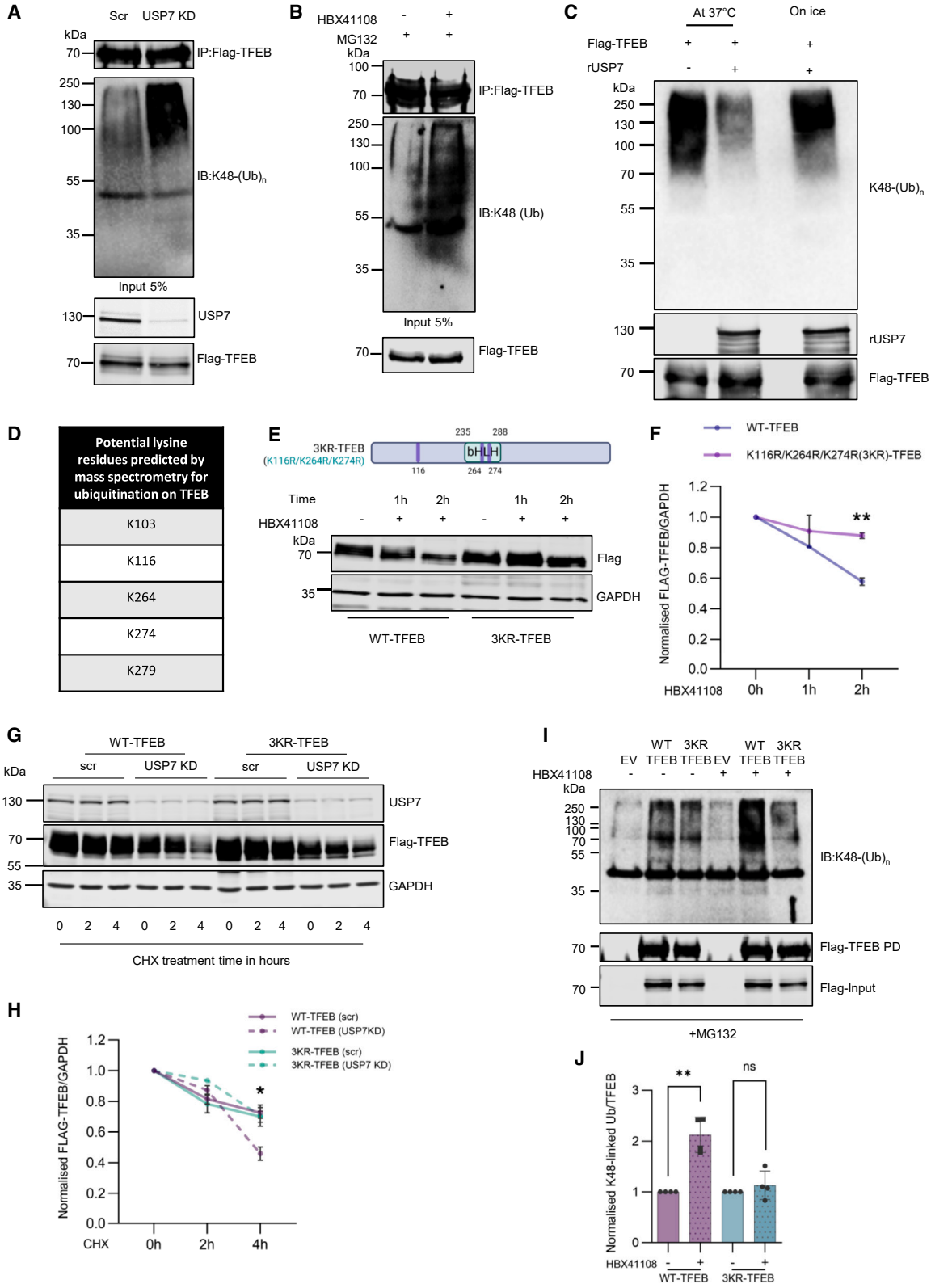

(legend on next page)

experiments of TFEB and TFE3, which resulted in a reduction in USP7 transcript levels (Figure S4B). Additionally, overexpression of WT and constitutively active TFEB (S211A-TFEB) led to a significant increase in USP7 transcript levels, reinforcing the positive regulatory role of TFEB in USP7 expression (Figure S4C).

To determine whether *USP7* is a direct target of TFEB, we performed chromatin IP (ChIP) assays under conditions of Torin 1 treatment and amino acid starvation, both of which are known to activate TFEB and promote its binding to the promoters of target genes.[14] Despite our initial hypothesis that *USP7* might be a TFEB target gene involved in a positive feedback loop, our ChIP data did not confirm TFEB binding to the *USP7* promoter at the predicted coordinated lysosomal expression and regulation (CLEAR) sequence (Figures S5A–S5E). Consequently, we decided to discontinue this line of investigation. However, we do not exclude the possibility of an indirect mechanism underlying this observation.

TFEB is deubiquitinated by USP7 at K116, K264, and K274

Genetic depletion (Figure 3A) or chemical inhibition of USP7 (Figures 3B, S6, S7A, and S7B) resulted in an increase in the K48-linked polyubiquitination signal on TFEB, consistent with our hypothesis that USP7 was a deubiquitinase for TFEB, which we confirmed using an *in vitro* deubiquitination assay (Figure 3C, lane 2). A negative control using ice-cold reaction conditions did not produce an effect similar to that observed at the optimal temperature for USP7 enzymatic activity (Figure 3C, lane 3). Furthermore, a control reaction performed without USP7 showed no significant reduction in the K48-linked polyubiquitin signal after 1 h of incubation at 37°C, suggesting that there was no inadvertent loss of ubiquitin signal during this time (Figure 3C, lane 1).

Having elucidated the ability of USP7 to remove polyubiquitination from TFEB, our next aim was to identify the lysine residues that undergo this modification and are deubiquitinated by USP7. Although a previous study identified STUB1 as an E3 ligase, it did not identify lysine residues on TFEB, but recent investigations have highlighted K347 as a potential ubiquitination site on TFEB, as the authors describe increased acetylation and decreased ubiquitination at this residue following trichostatin A treatment.[41] We investigated PTMs on TFEB, particularly under USP7 inhibition, using MS analysis. Initial analysis indicated that K274 could be a possible ubiquitination site on TFEB in response to USP7 inhibition (Figure S6A). However, substituting K274 with arginine only provided partial resistance to USP7 inhibition.

Subsequent MS analysis, conducted under similar conditions, identified several potential ubiquitination sites on TFEB that were specific to USP7 inhibition. These sites included K103, K116, K264, K279, and K347 (Figures 3D, S6B, and S6C). To determine the functional significance of these residues, lysine-to-arginine mutants were created, and their stability was evaluated when subjected to USP7 inhibition conditions. Single mutants did not provide stability to TFEB. However, two double mutants, K116R/K274R-TFEB and K264R/K274R-TFEB, showed complete resistance to USP7 inhibition (Figures S7C–S7F). Combining lysine residues from these double mutants into a triple mutant (3KR-TFEB) rendered TFEB immune to degradation under USP7 inhibition (Figures 3E and 3F).

Furthermore, when USP7 was genetically depleted, WT-TFEB underwent accelerated degradation compared to controls, while the 3KR-TFEB mutant remained largely unaffected, thus validating its resistance to USP7 loss of function (Figures 3G and 3H). Interestingly, a single point mutant, K347R-TFEB, did not provide immunity to USP7 inhibition (Figures S7G and S7H). Moreover, USP7 inhibition increased K48-linked polyubiquitination of WT-TFEB but not 3KR-TFEB (Figures 3I and 3J). When comparing TFEB with other MiT/TFE transcription factors, it is worth noting that TFEB has a singular presence of K116, while K264 and K274 are conserved. This observation may

Figure 3. K48-linked polyubiquitination of TFEB accumulates upon USP7 depletion or inhibition

USP7 deubiquitinates TFEB at three lysine residues: K116, K264, and K274.

(A) HeLa cells were transfected with 50 nM USP7 siRNA (#2) for 48 h to knock down USP7, followed by FLAG-TFEB transfection for 24 h. On day 4, cells were treated with the proteasome inhibitor MG132 (10 μM) for 4 h before harvesting for IP. The representative western blot in lane 2 shows an increase in K48-linked polyubiquitin-specific signal upon USP7 depletion. $n = 3$.

(B) HeLa cells were transfected with FLAG-TFEB for 24 h, treated with MG132 as described above, and additionally treated with HBX41108 (5 μM) 2 h before harvesting for IP. The representative western blot in lane 2 shows an increase in the K48-linked polyubiquitin-specific signal upon USP7 inhibition. $n = 3$.

(C) In an *in vitro* deubiquitination reaction, active recombinant USP7 enzyme was added at 37°C. The enzyme cleaved K48-linked polyubiquitin chains from purified FLAG-TFEB within 1 h (lane 2), as shown by the reduction of the K48-linked polyubiquitin signal in the representative western blot compared to negative controls. $n = 3$.

(D) Summary of MS analysis of TFEB post-translational modifications (PTMs) identifying several potential ubiquitination sites on TFEB specific to USP7 inhibition, including K103, K116, K264, K279, and K347.

(E) HeLa cells overexpressing TFEB constructs (WT-TFEB and 3KR-TFEB) were treated with the USP7 inhibitor HBX41108 (5 μM) for 1 or 2 h.

(F) The graph shows that the degradation rate of 3KR-TFEB is significantly slower than that of WT-TFEB upon USP7 inhibition. Data in the graph are presented as normalized mean ± SEM, $n = 3$. $p = 0.0026$ (WT-TFEB vs. 3KR-TFEB), two-way ANOVA with Šídák's multiple-comparisons post-test.

(G and H) HeLa cells were transfected with 50 nM USP7 siRNA (#2) for 48 h to knock down USP7, followed by overexpression of WT-TFEB or 3KR-TFEB for the last 24 h. On day 3, cells were treated with 25 μg/mL CHX. The western blot shows that FLAG-TFEB degrades faster than 3KR-TFEB under USP7 KD conditions. Data in the graph are presented as normalized mean ± SEM, $n = 3$. $^{*}p < 0.05$ (WT-TFEB [USP7KD] vs. 3KR-TFEB [USP7 KD]), two-way ANOVA with Tukey's multiple-comparisons post-test.

(I and J) After USP7 inhibition, an increase in K48-linked polyubiquitin signal was observed for WT-TFEB (lane 5) but not for 3KR-TFEB (lane 6), as shown in (J). Data in the graph are presented as normalized mean ± SEM, $n = 4$. Paired two-tailed Student's t test, $^{**}p < 0.01$ (WT-TFEB; DMSO vs. HBX41108); ns, not significant (3KR-TFEB; DMSO vs. HBX41108). The schematic was created using BioRender.

See also Figures S6–S9.

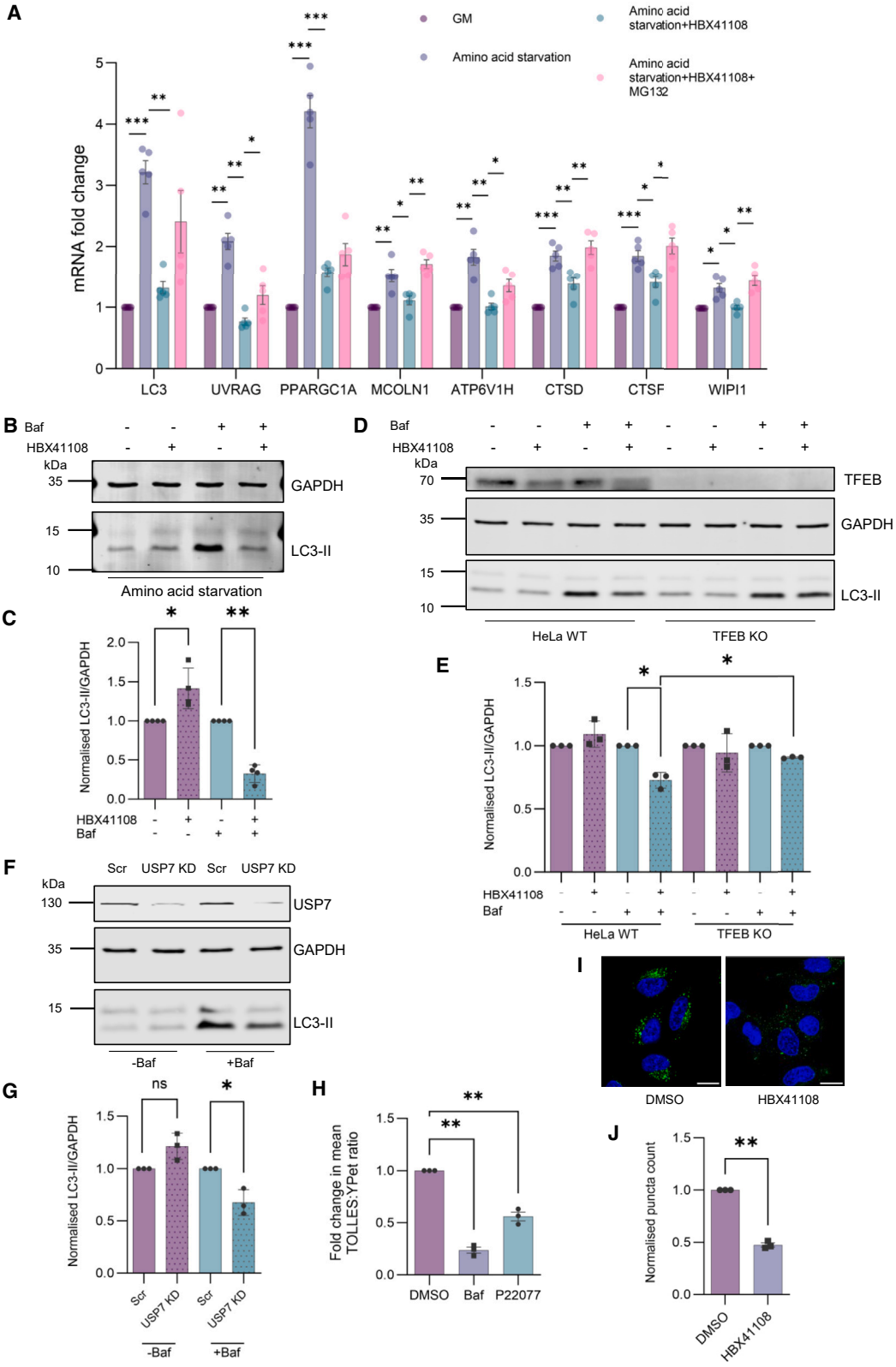

(legend on next page)

provide an explanation as to why TFEB is distinct from other members of the MiT/TFE family in its regulation by USP7 (Figures S7I and S8).

In summary, our findings highlight the crucial role of USP7 in deubiquitinating TFEB at K116, K264, and K274, thereby protecting it from proteasomal degradation.

USP7 plays a critical role in maintaining the TFEB-mediated transcription response to starvation and the autophagy flux

To elucidate the role of USP7 in TFEB-dependent transcription, we conducted an experiment incorporating four distinct conditions: (1) nutrient-rich growth medium (GM), (2) amino acid starvation, (3) amino acid starvation with the USP7 inhibitor HBX41108, and (4) amino acid starvation with both HBX41108 and the proteasomal inhibitor MG132.

We measured the mRNA levels of TFEB target genes, including *LC3B*. As expected, amino acid starvation resulted in a significant upregulation of these genes (Figure 4A). However, the presence of the USP7 inhibitor HBX41108 markedly suppressed this increase. Notably, the addition of MG132 reversed this suppression, restoring the expression of most TFEB target genes. These results suggest that USP7 inhibition leads to the destabilization of nuclear TFEB, promoting its proteasomal degradation and thereby diminishing its capacity to induce target gene expression under starvation conditions. The proteasomal inhibitor MG132 appears to rescue TFEB levels and its transcriptional activity.

Given the central role of TFEB in autophagy regulation, we aimed to investigate the downstream effects of USP7, a regulator of TFEB, on autophagy. Currently, only one study has reported an indirect link between USP7 and autophagy through SMAD2. In this study, USP7 was discovered to deubiquitinate the E3 ligase NEDD4L, resulting in its stabilization. This pathway facilitates the degradation of SMAD2, a transcription factor in the transforming growth factor β pathway and a positive regulator of autophagy, by NEDD4L.[42] However, we hypothesize that any effect observed on autophagy resulting from perturbations to the USP7-TFEB axis would manifest prior to the multi-step process proposed in the aforementioned report.

LC3, a widely recognized biochemical marker, was used to monitor autophagy flux. LC3-II levels correlate with autophagosome abundance; however, an increase in LC3-II can also occur due to autophagosome turnover blockade. LC3-II levels were assessed in conjunction with bafilomycin A1, an inhibitor of autophagosome-lysosome fusion or lysosomal acidification, to impede LC3-II degradation, which allows one to infer variations in LC3-II synthesis. Under conditions similar to those used for amino acid starvation transcription analysis, inhibiting USP7 in HeLa cells resulted in significantly lower levels of LC3-II in the presence of bafilomycin treatment (Figures 4B and 4C). This indicates defective autophagosome synthesis and autophagy induction. Similarly, autophagy induction was impaired when USP7 was inhibited under basal conditions. This experiment was performed in both WT and TFEB KO HeLa cell lines to determine the specificity of USP7 inhibition on autophagy and its mediation by TFEB. In WT HeLa cells, USP7 inhibition in the presence of bafilomycin consistently decreased LC3-II levels, suggesting decreased autophagosome biogenesis, but had little or no effect in TFEB KO cells (Figures 4D and 4E). This supports the idea that the USP7 inhibitor affects TFEB protein levels and, as a result, influences the autophagy pathway, since TFEB is one of its regulators. Furthermore, USP7 KD in bafilomycin-treated HEK293 cells resulted in a significant decrease in LC3-II levels, suggesting that autophagy induction is impaired upon USP7 KD, compatible with our inhibitor data in HeLa cells (Figures 4B–4E), and this was associated with reduced TFEB protein levels, as expected (Figures 4F, 4G, and S9A). In addition to the assays mentioned above, our group developed an advanced assay to monitor autophagy flux. This assay uses a fusion protein of the signal-retaining autophagy indicator (SRAI) reporter (a tandem fusion of the Ypet and TOLLES fluorescent proteins) and LC3B, a classical autophagy marker protein. After the protein is delivered to lysosomes via autophagy, the lysosome-sensitive Ypet protein is degraded, relieving fluorescence resonance energy transfer inhibition of the blue TOLLES signal (as TOLLES is relatively resistant to lysosomal proteolysis).[43] USP7 inhibition and our positive control bafilomycin decreased the TOLLES/Ypet ratio compared to the DMSO control, suggesting that autophagy flux is impaired, and autophagy substrates were degraded inefficiently by lysosomes (Figure 4H). This may be due to impaired lysosomal biogenesis as well as decreased autophagosome formation, as we demonstrated above. Furthermore, we observed a reduction in the number of

Figure 4. USP7 is essential for maintaining TFEB-mediated transcriptional response to starvation and autophagy flux

(A) HeLa cells were incubated with growth medium (GM) or an amino acid starvation medium, with or without the USP7 inhibitor HBX41108 (5 μM) and with or without the proteasome inhibitor MG132 for 6 h. The cells were then harvested for RNA isolation and RT-PCR analysis. The graph shows the mRNA fold change of various TFEB target genes in response to starvation, with and without USP7 inhibition, and the rescue effect of MG132 on USP7 inhibition. $n = 5$.

(B and C) HeLa cells were treated with amino acid starvation medium and HBX41108 (5 μM) for 6 h. Bafilomycin A1 (Baf; 400 nM) was added for the last 4 h. The representative western blot shows a significant reduction in LC3-II levels upon USP7 inhibition in the presence of Baf treatment. $n = 4$.

(D and E) WT and TFEB KO HeLa cells were treated with HBX41108 (5 μM) for 6 h (in GM), with Baf (400 nM) added for the last 4 h. The representative western blot demonstrates a marked reduction in LC3-II levels following USP7 inhibition in the presence of Baf treatment in WT HeLa cells but not in TFEB KO HeLa cells. $n = 3$.

(F and G) HEK293 cells were transfected with 50 nM USP7 siRNA (#2) for 48 h to knock down USP7. On day 3, cells were treated with Baf in GM. The representative western blot shows a significant reduction in LC3-II levels upon USP7 KD in the presence of Baf treatment. $n = 3$.

(H) The SRAI-LC3B HeLa reporter cell line was treated with the USP7 inhibitor P22077 (10 μM) or Baf (100 nM) for 24 h, resulting in a reduced fold change in the TOLLES/Ypet ratio. $n = 3$.

(I and J) HeLa cells were treated with the USP7 inhibitor HBX41108 (5 μM) for 6 h. Microscopy images were acquired using live cells stained with LysoTracker Green. The graph shows a decrease in LysoTracker-positive puncta upon USP7 inhibition. $n = 3$. Scale bars: 20 μM. Data in the graphs are presented as normalized mean ± SEM.

For all graphs, paired two-tailed Student's t test, $^{***}p < 0.001$, $^{**}p < 0.005$, $^{*}p < 0.05$ (DMSO vs. various conditions). See also Figure S9.

LysoTracker-positive puncta following USP7 inhibition (Figures 4I and 4J). Based on our observations, we propose that USP7 affects TFEB stability and thereby regulates genes involved in different stages of autophagosome and lysosomal biogenesis, which, in turn, impacts autophagy flux.

We examined the effects of the 3KR-TFEB mutant that is resistant to USP7 inhibition. This mutant appeared to have higher levels when expressed alongside its WT counterpart in normal cells, likely because it is resistant to ubiquitination (Figure S9B). Unexpectedly, the ChIP experiment data revealed that the 3KR mutant displayed reduced binding to TFEB target genes compared to WT-TFEB (Figure S9C). We hypothesize that the mutation of lysine residues K274, located at the TFEB dimer interface, and K264, which is in proximity to K274, may slightly impair dimerization, thereby leading to decreased chromatin binding and reduced affinity for TFEB target gene promoters.[17]

However, when we reconstituted a TFEB KO HeLa cell line with an empty vector, WT-TFEB, and 3KR-TFEB and assessed the steady-state levels of several TFEB target genes, the results indicated a significant upregulation, with 3KR-TFEB exhibiting a notably stronger response (Figure S9D). Thus, it is likely that the greater stability of the TFEB-3KR mutant relative to WT-TFEB outbalances its impaired chromatin binding, making it a stronger transcriptional inducer overall.

These findings underscore the critical role of USP7 in regulating TFEB stability and its downstream impact on autophagy, highlighting the complex interplay between protein deubiquitination and transcriptional control in cellular homeostasis.

DISCUSSION

Our investigation into the protein-protein interaction network of TFEB highlights the importance of understanding its regulatory intricacies, particularly in the context of amino acid starvation. This study aimed to address the paucity of data on TFEB regulation independent of its subcellular localization while also investigating mechanisms beyond its nuclear translocation; i.e., those governing TFEB turnover and stability.

Our research has uncovered the role of the deubiquitinase USP7 as a modulator of TFEB. We have shown that USP7-mediated deubiquitination at specific lysine residues—namely, K116, K264, and K274—stabilizes TFEB, prevents its proteasomal degradation, and, consequently, affects its transcriptional activity. Our results suggest that USP7-mediated deubiquitination serves as a critical mechanism to control TFEB activity, particularly in response to starvation-induced signaling. Interestingly, two of the three lysine residues, K116 and K274, have been reported previously to be acetylated.[17] This provides an opportunity to explore a paradigm of crosstalk between two PTMs, ubiquitination and acetylation, to control the activity of TFEB.

Furthermore, our study highlights the potential therapeutic implications of targeting USP7 in diseases characterized by dysregulated TFEB activity. In conditions where TFEB is hyperactivated and constitutively localized to the nucleus, such as Birt-Hogg-Dubé syndrome, exploring USP7 inhibition as a therapeutic strategy may lower nuclear TFEB levels and activity, potentially attenuating tumorigenesis.[12] Conversely, exogenous expression of USP7 may counteract TFEB degradation and preserve its activity in scenarios where TFEB turnover is accelerated, such as Gaucher disease.[44]

Moreover, the elevated expression of *USP7* in various cancers, such as breast, prostate, colorectal, and lung cancer, underscores its central role in tumorigenesis.[45–48] As a post-translational modifier, USP7 controls cellular pathways that promote cancer progression, including increased proliferation, evasion of growth-suppressive signals, inhibition of apoptosis, and maintenance of genomic instability.[49] A prominent avenue for pharmacological targeting of USP7 has shown potential in promoting p53-mediated cell-cycle arrest and apoptosis, positioning USP7 as an attractive therapeutic target.[50,51] However, the heterogeneous substrate spectrum of USP7, which includes both tumor suppressor and oncogenic elements, requires careful investigation. Our study highlights the importance of studying the USP7-TFEB axis and its potential to provide critical insights into the mechanisms by which USP7 affects metabolic reprogramming of cancer cells and, thereby, cancer progression. This may be by stabilizing TFEB and its subsequent regulation of cancer cell metabolism.[52]

Limitations of the study

Our studies were performed in cell culture. Thus, it would be interesting to understand the roles of USP7 *in vivo* in different tissues exposed to starvation for different periods. As with most loss-of-function studies, it would be informative to understand the magnitudes of USP7 reductions that impact TFEB and its downstream processes. However, since USP7 overexpression resulted in increased TFEB levels, it is likely that USP7 activity alterations above and below the normal physiological levels impact TFEB. The residual K48-linked ubiquitination observed in the 3KR mutant suggests other ubiquitination sites on TFEB that are not deubiquitinated by USP7, though the functional significance of these sites remains unclear. We also did not fully explore how the endogenous ubiquitinated versus deubiquitinated forms of TFEB affect chromatin binding and transcriptional regulation. Finally, while our data suggest that USP7 transcription is TFEB dependent, this regulation does not appear to involve canonical TFEB-binding motifs in the USP7 promoter. The underlying mechanisms and the impact of varying USP7 levels on TFEB function *in vivo*, particularly in different tissues under starvation conditions, remain to be elucidated.

RESOURCE AVAILABILITY

Lead contact

Requests for further information, resources, and reagents should be directed to and will be fulfilled by the lead contact, David Rubinsztein (dcr1000@cam.ac.uk).

Materials availability

The plasmids generated in this study are available upon request.

Data and code availability

- The MS proteomics data have been deposited in the ProteomeXchange Consortium via the PRIDE partner repository with the dataset identifier PXD055937. Original western blot images and microscopy data reported in this paper will be shared by the lead contact upon request.
- This paper does not report original code.

- Any additional information required to reanalyze the data reported in this paper is available from the lead contact upon request.

ACKNOWLEDGMENTS

We are grateful for funding from the UK Dementia Research Institute, through UK DRI Ltd., principally funded by the Medical Research Council, and the NIHR Cambridge Biomedical Research Centre (BRC-1215-20014). S.K. is funded by the Cambridge Commonwealth, European & International Trust, the Nehru Trust for Cambridge University, and the Trinity-Henry Barlow Scholarship. M.T. is funded by the Rosetrees Trust and the Cambridge University School of Clinical Medicine (James Baird Fund and F.E. Elmore Fund). The views expressed are those of the authors and not necessarily those of the NIHR or the Department of Health and Social Care. We are grateful to Dr. Lidia Wrobel for her help and guidance with the ubiquitination-related assays as well as for her support with troubleshooting. We would like to express our sincerest gratitude to the CIMR Proteomics Facility (CIPF) and Dr. Robin Antrobus for conducting the mass spectrometry experiments and assisting us with data analysis and deposition into a public access repository. Additionally, we would like to acknowledge Douglas Lamont, the Proteomics Facility Manager at the "FingerPrints" Proteomics Facility, University of Dundee, for his significant contribution to identifying post-translational modifications through mass spectrometry. Furthermore, we would like to express our gratitude to the CIMR Flow Cytometry Core Facility and Microscopy Facility for their guidance and support in conducting the experiments presented in this paper.

AUTHOR CONTRIBUTIONS

Conceptualization, D.C.R., S.K., and M.V.; methodology, S.K. and M.V.; investigation, S.K. and M.T.; writing – original draft, S.K.; writing – review & editing, S.K. and D.C.R.; funding acquisition, D.C.R.; resources, S.K. and D.C.R.; supervision, D.C.R. and M.V.

DECLARATION OF INTERESTS

D.C.R. is a consultant for Aladdin Healthcare Technologies Ltd., Mindrank AI, Nido Biosciences, Drishti Discoveries, Retro Biosciences, PAQ Therapeutics, and Alexion Pharma International Operations Limited. M.V. is currently employed by GlaxoSmithKline.

STAR★METHODS

Detailed methods are provided in the online version of this paper and include the following:

- KEY RESOURCES TABLE
- EXPERIMENTAL MODEL AND STUDY PARTICIPANT DETAILS
  - Cell culture
- METHOD DETAILS
  - Transient transfection
  - GFP trap for mass spectrometry experiment
  - LC-MS/MS
  - Immunofluorescence
  - Proximity ligation assay (PLA)
  - Immunoprecipitation
  - Western blotting
  - Purification of ubiquitinated Flag-TFEB protein
  - *In vitro* DUB assay
  - Site-directed mutagenesis for point mutations
  - Isolation of RNA and RT-PCR
  - Flow cytometry
  - Lysotracker staining
  - Chromatin immunoprecipitation (ChIP) assay
- QUANTIFICATION AND STATISTICAL ANALYSIS

SUPPLEMENTAL INFORMATION

Supplemental information can be found online at https://doi.org/10.1016/j.celrep.2024.114872.

Received: April 25, 2024
Revised: August 22, 2024
Accepted: September 27, 2024
Published: October 16, 2024

REFERENCES

1. La Spina, M., Contreras, P.S., Rissone, A., Meena, N.K., Jeong, E., and Martina, J.A. (2020). MiT/TFE Family of Transcription Factors: An Evolutionary Perspective. Front. Cell Dev. Biol. *8*, 609683. https://doi.org/10.3389/fcell.2020.609683.
2. Fisher, D.E., Carr, C.S., Parent, L.A., and Sharp, P.A. (1991). TFEB has DNA-binding and oligomerization properties of a unique helix-loop-helix/leucine-zipper family. Genes Dev. *5*, 2342–2352. https://doi.org/10.1101/GAD.5.12A.2342.
3. Palmieri, M., Impey, S., Kang, H., di Ronza, A., Pelz, C., Sardiello, M., and Ballabio, A. (2011). Characterization of the CLEAR network reveals an integrated control of cellular clearance pathways. Hum. Mol. Genet. *20*, 3852–3866. https://doi.org/10.1093/HMG/DDR306.
4. Settembre, C., Di Malta, C., Polito, V.A., Garcia Arencibia, M., Vetrini, F., Erdin, S., Erdin, S.U., Huynh, T., Medina, D., Colella, P., et al. (2011). TFEB Links Autophagy to Lysosomal Biogenesis. Science *332*, 1429–1433. https://doi.org/10.1126/science.1204592.
5. Sardiello, M., Palmieri, M., di Ronza, A., Medina, D.L., Valenza, M., Gennarino, V.A., Di Malta, C., Donaudy, F., Embrione, V., Polishchuk, R.S., et al. (2009). A gene network regulating lysosomal biogenesis and function. Science *325*, 473–477. https://doi.org/10.1126/SCIENCE.1174447.
6. Martina, J.A., and Puertollano, R. (2018). Protein phosphatase 2A stimulates activation of TFEB and TFE3 transcription factors in response to oxidative stress. J. Biol. Chem. *293*, 12525–12534. https://doi.org/10.1074/JBC.RA118.003471.
7. Martina, J.A., Diab, H.I., Brady, O.A., and Puertollano, R. (2016). TFEB and TFE 3 are novel components of the integrated stress response. EMBO J. *35*, 479–495. https://doi.org/10.15252/embj.201593428.
8. Brady, O.A., Jeong, E., Martina, J.A., Pirooznia, M., Tunc, I., and Puertollano, R. (2018). The transcription factors TFE3 and TFEB amplify p53 dependent transcriptional programs in response to DNA damage. Elife *7*, e40856. https://doi.org/10.7554/ELIFE.40856.
9. Nezich, C.L., Wang, C., Fogel, A.I., and Youle, R.J. (2015). MiT/TFE transcription factors are activated during mitophagy downstream of Parkin and Atg5. J. Cell Biol. *210*, 435–450. https://doi.org/10.1083/jcb.201501002.
10. Roczniak-Ferguson, A., Petit, C.S., Froehlich, F., Qian, S., Ky, J., Angarola, B., Walther, T.C., and Ferguson, S.M. (2012). The transcription factor TFEB links mTORC1 signaling to transcriptional control of lysosome homeostasis. Sci. Signal. *5*, ra42. https://doi.org/10.1126/SCISIGNAL.2002790.
11. Vega-Rubin-de-Celis, S., Peña-Llopis, S., Konda, M., and Brugarolas, J. (2017). Multistep regulation of TFEB by MTORC1. Autophagy *13*, 464–472. https://doi.org/10.1080/15548627.2016.1271514.
12. Napolitano, G., Di Malta, C., Esposito, A., de Araujo, M.E.G., Pece, S., Bertalot, G., Matarese, M., Benedetti, V., Zampelli, A., Stasyk, T., et al. (2020). A substrate-specific mTORC1 pathway underlies Birt–Hogg–Dubé syndrome. Nature *585*, 597–602. https://doi.org/10.1038/s41586-020-2444-0.
13. Peña-Llopis, S., Vega-Rubin-De-Celis, S., Schwartz, J.C., Wolf, N.C., Tran, T.A., Zou, L., Xie, X.J., Corey, D.R., and Brugarolas, J. (2011). Regulation of TFEB and V-ATPases by mTORC1. EMBO J. *30*, 3242–3258. https://doi.org/10.1038/EMBOJ.2011.257.

14. Settembre, C., Zoncu, R., Medina, D.L., Vetrini, F., Erdin, S., Erdin, S., Huynh, T., Ferron, M., Karsenty, G., Vellard, M.C., et al. (2012). A lysosome-to-nucleus signalling mechanism senses and regulates the lysosome via mTOR and TFEB. EMBO J. *31*, 1095–1108. https://doi.org/10.1038/EMBOJ.2012.32.

15. Martina, J.A., and Puertollano, R. (2013). Rag GTPases mediate amino acid-dependent recruitment of TFEB and MITF to lysosomes. J. Cell Biol. *200*, 475–491. https://doi.org/10.1083/jcb.201209135.

16. Miller, A.J., Levy, C., Davis, I.J., Razin, E., and Fisher, D.E. (2005). Sumoylation of MITF and its related family members TFE3 and TFEB. J. Biol. Chem. *280*, 146–155. https://doi.org/10.1074/JBC.M411757200.

17. Wang, Y., Huang, Y., Liu, J., Zhang, J., Xu, M., You, Z., Peng, C., Gong, Z., and Liu, W. (2020). Acetyltransferase GCN5 regulates autophagy and lysosome biogenesis by targeting TFEB. EMBO Rep. *21*, e48335. https://doi.org/10.15252/EMBR.201948335.

18. Sha, Y., Rao, L., Settembre, C., Ballabio, A., and Eissa, N.T. (2017). STUB 1 regulates TFEB -induced autophagy–lysosome pathway. EMBO J. *36*, 2544–2552. https://doi.org/10.15252/EMBJ.201796699.

19. Song, W., Wang, F., Savini, M., Ake, A., di Ronza, A., Sardiello, M., and Segatori, L. (2013). TFEB regulates lysosomal proteostasis. Hum. Mol. Genet. *22*, 1994–2009. https://doi.org/10.1093/HMG/DDT052.

20. Napolitano, G., and Ballabio, A. (2016). CELL SCIENCE AT A GLANCE TFEB at a glance. J. Cell Sci. *129*, 2475–2481, Published online. https://doi.org/10.1242/jcs.146365.

21. Gu, Z., Cao, H., Zuo, C., Huang, Y., Miao, J., Song, Y., Yang, Y., Zhu, L., and Wang, F. (2022). TFEB in Alzheimer's disease: From molecular mechanisms to therapeutic implications. Neurobiol. Dis. *173*, 105855. https://doi.org/10.1016/J.NBD.2022.105855.

22. Kauffman, E.C., Ricketts, C.J., Rais-Bahrami, S., Yang, Y., Merino, M.J., Bottaro, D.P., Srinivasan, R., and Linehan, W.M. (2014). Molecular genetics and cellular features of TFE3 and TFEB fusion kidney cancers. Nat. Rev. Urol. *11*, 465–475. https://doi.org/10.1038/nrurol.2014.162.

23. Cortes, C.J., Miranda, H.C., Frankowski, H., Batlevi, Y., Young, J.E., Le, A., Ivanov, N., Sopher, B.L., Carromeu, C., Muotri, A.R., et al. (2014). Polyglutamine-expanded androgen receptor interferes with TFEB to elicit autophagy defects in SBMA. Nat. Neurosci. *17*, 1180–1189, Published online. https://doi.org/10.1038/nn.3787.

24. Evans, T.D., Zhang, X., Jeong, S.J., He, A., Song, E., Bhattacharya, S., Holloway, K.B., Lodhi, I.J., and Razani, B. (2019). TFEB drives PGC-1α expression in adipocytes to protect against diet-induced metabolic dysfunction. Sci. Signal. *12*, eaau2281. https://doi.org/10.1126/SCISIGNAL.AAU2281.

25. Everett, R.D., Meredith, M., Orr, A., Cross, A., Kathoria, M., and Parkinson, J. (1997). A novel ubiquitin-specific protease is dynamically associated with the PML nuclear domain and binds to a herpesvirus regulatory protein. EMBO J. *16*, 1519–1530. https://doi.org/10.1093/EMBOJ/16.7.1519.

26. Valles, G.J., Bezsonova, I., Woodgate, R., and Ashton, N.W. (2020). USP7 Is a Master Regulator of Genome Stability. Front. Cell Dev. Biol. *8*. https://doi.org/10.3389/fcell.2020.00717.

27. Rawat, R., Starczynowski, D.T., and Ntziachristos, P. (2019). Nuclear deubiquitination in the spotlight: the multifaceted nature of USP7 biology in disease. Curr. Opin. Cell Biol. *58*, 85–94. https://doi.org/10.1016/J.CEB.2019.02.008.

28. Pozhidaeva, A., and Bezsonova, I. (2019). USP7: Structure, substrate specificity, and inhibition. DNA Repair *76*, 30–39. https://doi.org/10.1016/J.DNAREP.2019.02.005.

29. Fernández-Montalván, A., Bouwmeester, T., Joberty, G., Mader, R., Mahnke, M., Pierrat, B., Schlaeppi, J.-M., Worpenberg, S., and Gerhartz, B. (2007). Biochemical characterization of USP7 reveals post-translational modification sites and structural requirements for substrate processing and subcellular localization. FEBS J. *274*, 4256–4270. https://doi.org/10.1111/j.1742-4658.2007.05952.x.

30. Hu, M., Li, P., Li, M., Li, W., Yao, T., Wu, J.W., Gu, W., Cohen, R.E., and Shi, Y. (2002). Crystal structure of a UBP-family deubiquitinating enzyme in isolation and in complex with ubiquitin aldehyde. Cell *111*, 1041–1054. https://doi.org/10.1016/S0092-8674(02)01199-6.

31. Faesen, A.C., Dirac, A.M.G., Shanmugham, A., Ovaa, H., Perrakis, A., and Sixma, T.K. (2011). Mechanism of USP7/HAUSP activation by its C-Terminal ubiquitin-like domain and allosteric regulation by GMP-synthetase. Mol. Cell *44*, 147–159. https://doi.org/10.1016/J.MOLCEL.2011.06.034.

32. Ji, L., Lu, B., Zamponi, R., Charlat, O., Aversa, R., Yang, Z., Sigoillot, F., Zhu, X., Hu, T., Reece-Hoyes, J.S., et al. (2019). USP7 inhibits Wnt/β-catenin signaling through promoting stabilization of Axin. Nat. Commun. *10*, 4184. https://doi.org/10.1038/s41467-019-12143-3.

33. Li, M., Brooks, C.L., Kon, N., and Gu, W. (2004). A dynamic role of HAUSP in the p53-Mdm2 pathway. Mol. Cell *13*, 879–886. https://doi.org/10.1016/S1097-2765(04)00157-1.

34. Pickart, C.M. (2001). Mechanisms Underlying Ubiquitination. Annu. Rev. Biochem. *70*, 503–533. https://doi.org/10.1146/ANNUREV.BIOCHEM.70.1.503.

35. Voges, D., Zwickl, P., and Baumeister, W. (1999). The 26S Proteasome: A Molecular Machine Designed for Controlled Proteolysis. Annu. Rev. Biochem. *68*, 1015–1068. https://doi.org/10.1146/ANNUREV.BIOCHEM.68.1.1015.

36. BROOKS, P., FUERTES, G., MURRAY, R.Z., Bose, S., Knecht, E., Rechsteiner, M.C., Hendil, K.B., Tanaka, K., Dyson, J., and Rivett, J. (2000). Subcellular localization of proteasomes and their regulatory complexes in mammalian cells. Biochem. J. *346 Pt 1*, 155–161. https://doi.org/10.1042/BJ3460155.

37. Scharf, A., Rockel, T.D., and Von Mikecz, A. (2007). Localization of proteasomes and proteasomal proteolysis in the mammalian interphase cell nucleus by systematic application of immunocytochemistry. Histochem. Cell Biol. *127*, 591–601. https://doi.org/10.1007/S00418-006-0266-2/FIGURES/6.

38. Yang, S., Ting, C.Y., and Lilly, M.A. (2024). The GATOR2 complex maintains lysosomal-autophagic function by inhibiting the protein degradation of MiT/TFEs. Mol. Cell *84*, 727–743.e8. https://doi.org/10.1016/j.molcel.2024.01.012.

39. Canning, M., Boutell, C., Parkinson, J., and Everett, R.D. (2004). A RING finger ubiquitin ligase is protected from autocatalyzed ubiquitination and degradation by binding to ubiquitin-specific protease USP7. J. Biol. Chem. *279*, 38160–38168. https://doi.org/10.1074/jbc.M402885200.

40. Martina, J.A., Chen, Y., Gucek, M., and Puertollano, R. (2012). MTORC1 functions as a transcriptional regulator of autophagy by preventing nuclear transport of TFEB. Autophagy *8*, 903–914. https://doi.org/10.4161/AUTO.19653.

41. Li, T., Yin, L., Kang, X., Xue, W., Wang, N., Zhang, J., Yuan, P., Lin, L., and Li, Y. (2022). TFEB acetylation promotes lysosome biogenesis and ameliorates Alzheimer's disease-relevant phenotypes in mice. J. Biol. Chem. *298*, 102649. https://doi.org/10.1016/j.jbc.2022.102649.

42. Zhang, T., Periz, G., Lu, Y.N., and Wang, J. (2020). USP7 regulates ALS-associated proteotoxicity and quality control through the NEDD4L-SMAD pathway. Proc. Natl. Acad. Sci. USA *117*, 28114–28125. https://doi.org/10.1073/PNAS.2014349117.

43. Wrobel, L., Hill, S.M., Djajadikerta, A., Fernandez-Estevez, M., Karabiyik, C., Ashkenazi, A., Barratt, V.J., Stamatakou, E., Gunnarsson, A., Rasmusson, T., et al. (2022). Compounds activating VCP D1 ATPase enhance both autophagic and proteasomal neurotoxic protein clearance. Nat. Commun. *13*, 4146–4219. https://doi.org/10.1038/s41467-022-31905-0.

44. Awad, O., Sarkar, C., Panicker, L.M., Miller, D., Zeng, X., Sgambato, J.A., Lipinski, M.M., and Feldman, R.A. (2015). Altered TFEB-mediated lysosomal biogenesis in Gaucher disease iPSC-derived neuronal cells. Hum. Mol. Genet. *24*, 5775–5788. https://doi.org/10.1093/HMG/DDV297.

45. Zhao, G.Y., Lin, Z.W., Lu, C.L., Gu, J., Yuan, Y.F., Xu, F.K., Liu, R.H., Ge, D., and Ding, J.Y. (2015). USP7 overexpression predicts a poor prognosis in lung squamous cell carcinoma and large cell carcinoma. Tumor Biol. *36*, 1721–1729. https://doi.org/10.1007/S13277-014-2773-4.

46. Basu, B., Karmakar, S., Basu, M., and Ghosh, M.K. (2023). USP7 imparts partial EMT state in colorectal cancer by stabilizing the RNA helicase DDX3X and augmenting Wnt/β-catenin signaling. Biochim. Biophys. Acta Mol. Cell Res. *1870*, 119446. https://doi.org/10.1016/J.BBAMCR.2023.119446.

47. Song, M.S., Salmena, L., Carracedo, A., Egia, A., Lo-Coco, F., Teruya-Feldstein, J., and Pandolfi, P.P. (2008). The deubiquitinylation and localization of PTEN are regulated by a HAUSP–PML network. Nature *455*, 813–817. https://doi.org/10.1038/nature07290.

48. Wang, Q., Ma, S., Song, N., Li, X., Liu, L., Yang, S., Ding, X., Shan, L., Zhou, X., Su, D., et al. (2016). Stabilization of histone demethylase PHF8 by USP7 promotes breast carcinogenesis. J. Clin. Invest. *126*, 2205–2220. https://doi.org/10.1172/JCI85747.

49. Saha, G., Roy, S., Basu, M., and Ghosh, M.K. (2023). USP7 - a crucial regulator of cancer hallmarks. Biochim. Biophys. Acta Rev. Canc *1878*, 188903. https://doi.org/10.1016/j.bbcan.2023.188903.

50. Fan, Y.H., Cheng, J., Vasudevan, S.A., Dou, J., Zhang, H., Patel, R.H., Ma, I.T., Rojas, Y., Zhao, Y., Yu, Y., et al. (2013). USP7 inhibitor P22077 inhibits neuroblastoma growth via inducing p53-mediated apoptosis. Cell Death Dis. *4*, e867. https://doi.org/10.1038/CDDIS.2013.400.

51. Dar, A., Shibata, E., and Dutta, A. (2013). Deubiquitination of Tip60 by USP7 Determines the Activity of the p53-Dependent Apoptotic Pathway. Mol. Cell Biol. *33*, 3309–3320. https://doi.org/10.1128/MCB.00358-13.

52. Hall, J.A., Tabata, M., Rodgers, J.T., and Puigserver, P. (2014). USP7 Attenuates Hepatic Gluconeogenesis Through Modulation of FoxO1 Gene Promoter Occupancy. Mol. Endocrinol. *28*, 912–924. https://doi.org/10.1210/ME.2013-1420.

53. Ashton, N.W., Valles, G.J., Jaiswal, N., Bezsonova, I., and Woodgate, R. (2021). DNA Polymerase ι Interacts with Both the TRAF-like and UBL1-2 Domains of USP7. J. Mol. Biol. *433*, 166733. https://doi.org/10.1016/J.JMB.2020.166733.

STAR★METHODS

KEY RESOURCES TABLE

REAGENT or RESOURCE	SOURCE	IDENTIFIER
Antibodies		
Actin	Sigma-Aldrich	Rabbit; Polyclonal; Cat#A2066; RRID: AB_476693
ANTIFLAG®	Sigma-Aldrich	Mouse; M2 mAb; Cat#F3165; RRID: AB_259529
DyLight 680	Thermo Fisher Scientific	Anti-Rabbit; Cat#355568; RRID:AB_614946
DyLight 800	Thermo Fisher Scientific	Anti-mouse; Cat#SA535521; RRID:AB_2556616
GAPDH	Abcam	Mouse; 6C5; Cat#ab8245; RRID: AB_2107448
GAPDH	Cell Signaling	Rabbit; 14C10 mAb; Cat#2118; RRID: AB_561053
IgG	Cell Signaling	Rabbit; Polyclonal; Cat#2729; RRID: AB_1031062
K48 Ub	Cell Signaling	Rabbit; D9D5 mAb; Cat#8081; RRID: AB_10859893
Lamin B1	Abcam	Rabbit; Polyclonal; Cat# ab65986
LC3B	Abcam	Rabbit; Polyclonal; Cat#ab192890; RRID: AB_2827794
Myc	Abcam	Rabbit; Polyclonal; Cat#ab9106; RRID: AB_307014
Myc	Proteintech	Mouse; 1A5A2 mAb; Cat#60003-2-Ig; RRID: AB_2734122
STUB1	Abcam	Rabbit; Monoclonal; Cat# ab134064; RRID: AB_2751008
TFEB	Cell Signaling	Rabbit; Polyclonal; Cat#4240; RRID: AB_11220225
TFE3	Cell Signaling	Rabbit; Polyclonal; Cat#14779; RRID: AB_2687582
USP7	Bethyl Laboratories	Rabbit; Polyclonal; Cat#A300-034A; RRID: AB_203277
Goat anti-Mouse IgG (H + L), Alexa Fluor 488	Invitrogen	Cat# A-11001
Goat anti-Mouse IgG (H + L), Alexa Fluor 555	Invitrogen	Cat# A-21422
HRP-conjugated ECL secondary	GE Healthcare	Anti-Rabbit; Cat#NA934
Chemicals, peptides, and recombinant proteins		
Bafilomycin A1	Enzo	Cat#BML-CM110
Cycloheximide	Sigma-Aldrich	Cat#C7698
PR 619	Abcam	Cat#ab144641
Dynabeads Protein A	Invitrogen	Cat#10002D
HBX41108	Tocris	Cat#4285
MG132	Sigma	Cat#C2211
P22077	Merck (Calbiochem)	Cat#662142
P005091	MedChemExpress	Cat# HY-15667
XL177A	MedChemExpress	Cat# HY-138794
PureBlu™ Hoechst 33342 Dye	BIO-RAD	Cat#135-1304
Recombinant USP7	2Bscientific (Lifesensors)	Cat# DB502: USP7
Torin 1	Tocris	Cat#4247
Poly-D-Lysine	Sigma-Aldrich	Cat#P6407
Bovine Serum Albumin	Sigma-Aldrich	Cat#A9418
Paraformaldehyde	Sigma-Aldrich	Cat# 158127
DAPI	Invitrogen	Cat# P36981
cOmplete™ Protease Inhibitor Cocktail	Roche	Cat# 11697498001
DTT	Roche	Cat# 10708984001
Triton® X-100	Merck	Cat# 112298
DMEM	Sigma-Aldrich	Cat#D6429
EBSS	Sigma-Aldrich	Cat#E2888

(*Continued on next page*)

Continued

REAGENT or RESOURCE	SOURCE	IDENTIFIER
Penicillin/Streptomycin	Sigma-Aldrich	Cat#P0781
Fetal Bovine Serum	Sigma-Aldrich	Cat#F7524
MEM Essential Amino Acid (50X)	Merck	Cat#M5550
MEM Non-Essential Amino Acid (100X)	Merck	Cat#M7145
Dialyzed FBS	Thermo Fisher Scientific	Cat#A3382001
GlutaMAX	Invitrogen	Cat#35050061
Amino acid free DMEM	USBiological	Cat#D9800-13
TransIT-2020 Transfection Reagent	Mirus	Cat# E7-0148
Lipofectamine™ 2000 Transfection reagent	Thermo Fisher Scientific	Cat# 11668019
Sodium bicarbonate	Sigma-Aldrich	Cat#S6014
Glucose	Sigma-Aldrich	Cat#SLBN1246V
Critical commercial assays		
Duolink® PLA fluorescence kit (red)	Sigma-Aldrich	Cat#DUO92008
GFP-Trap® Magnetic Agarose	ChromoTek	RRID# AB_2631358
Anti-FLAG® M2 magnetic Beads	Merck	Cat#M8823
LysoTracker™ Green DND-26	Thermo Fisher Scientific	Cat# L7526
PureLink™ HiPure Plasmid Filter Maxiprep Kit	Invitrogen	Cat#K210006
RNeasy Mini Kit	QIAGEN	Cat# 74104
QIAprepSpin Miniprep Kits	QIAGEN	Cat#27106X4
QuickChange Lightning Site-Directed Mutagenesis Kit	Agilent Technologies	Cat#210518
NE-PER™ Nuclear and Cytoplasmic Extraction Reagents	Thermo Fisher Scientific	Cat# 78833
SimpleChIP® Plus Enzymatic Chromatin IP Kit	Cell Signaling	Cat# 9005
Luna® Universal One-Step RT-qPCR Kit	NEW ENGLAND Biolabs	Cat# E3005L
Deposited data		
Raw Mass Spectrometry Data Files	This paper	Data are available via ProteomeXchange with identifier PXD055937
Experimental models: Cell lines		
Human: HeLa cervical cancer cells	ATCC	Cat#CCL-2; CVCL_0030
Human embryonic kidney cell line HEK-293T cells	ECACC	Cat# #85120602
Human USP7 (HAUSP) knockout HEK-293T cell line	Abcam	Cat# ab266535
TFEB knockout HeLa cells	Gift from Richard J. Youle	N/A
TFEB/TFE3 or Double knockout HeLa cells	Gift from Richard J. Youle	N/A
Control HeLa WT cells	Gift from Richard J. Youle	N/A
HeLa-SRAI-LC3B	Wrobel et al.[43]	N/A
Oligonucleotides		
Sequence of siRNAs used in this study, see Table S2	Dharmacon	Refer to Table S2 for further details
Primers used in this study, see Tables S3–S5	This study	N/A
Recombinant DNA		
pcDNA3.1(−), Empty vector	Invitrogen	Cat#V79520
pcDNA3.1-N-Myc_WT USP7	Ashton et al.[53]	Addgene #131242; RRID:Addgene_131242

(*Continued on next page*)

Continued

REAGENT or RESOURCE	SOURCE	IDENTIFIER
pcDNA3.1-N-Myc_C223S USP7	Ashton et al.[53]	Addgene#131243; RRID:Addgene_131243
pCMV6-FLAG-Myc	Origene	PS100001
pCMV TFEB WT 3xFlag	Gift from A. Ballabio	N/A
pEGFP-N1-TFEB	Settembre et al.[4]	Addgene#38119; RRID:Addgene_38119
pEGFP-C1	Clontech	#6084-1
pCMV K116R/K264R/K274R-TFEB 3xFlag	This study	N/A
pCMV K116R/K274R-TFEB 3xFlag	This study	N/A
pCMV K264R/K274R-TFEB 3xFlag	This study	N/A
pCMV K274R-TFEB 3xFlag	This study	N/A
pCMV K347R-TFEB 3xFlag	This study	N/A
pcDNA3.1-TFEB-WT-MYC (#647)	Vega-Rubin-de-Celis et al.[11]	Addgene#99955; RRID:Addgene_99955
pCMV TFEB S142A 3xFlag	Gift from A. Ballabio	N/A
pcDNA3.1-TFEBS211A-MYC (#805)	Vega-Rubin-de-Celis et al.[11]	Addgene#99957; RRID:Addgene_99957
pcDNA3.1-TFEBS122D-MYC (#777)	Vega-Rubin-de-Celis et al.[11]	Addgene#99956; RRID:Addgene_99956
Software and algorithms		
GraphPad Prism 10	GraphPad	https://www.graphpad.com/
BioRender	BioRender	https://www.biorender.com/
ImageJ software	GitHub	https://imagej.net
Image Studio software	LI-COR	https://www.licor.com/bio/image-studio/
Scaffold	Proteome software	https://www.proteomesoftware.com/

EXPERIMENTAL MODEL AND STUDY PARTICIPANT DETAILS

Cell culture

HeLa and HEK-293 cells were cultured in high-glucose DMEM supplemented with 100 U/ml pen/strep and 10% FBS at 37°C under a 5% CO_2 atmosphere. In preparation for starvation mass spectrometry experiments, cells were cultured in EBSS for the specified times. Refeeding was carried out using EBSS supplemented with 2X MEM essential amino acid and MEM nonessential amino acid solutions, 10% dialyzed FBS, and 2 mM GlutaMAX supplement. Amino acid starvation medium for RT-PCR experiments was prepared from amino acid-free DMEM powder, glucose, sodium bicarbonate, 100 U/ml pen/strep, and 10% dialyzed FBS. The control medium was supplemented with essential and non-essential amino acid solutions and GlutaMAX. Cells were passaged by trypsinisation when they reached 80–90% confluence. Only cells with passage numbers below 20 were used in the experiments to avoid potential artifacts caused by excessive growth time in culture. All cell lines underwent regular testing for mycoplasma contamination.

METHOD DETAILS

Transient transfection

HeLa cells were transiently transfected using a purified plasmid and the Mirus TransIT-2020 transfection reagent in penicillin/streptomycin-free DMEM medium. The plasmid DNA and TransIT-2020 reagent were diluted at a 1:3 ratio in opti-MEM, mixed, and incubated for 20-25 min to form DNA-lipid complexes. These complexes were then added to the HeLa cells and incubated overnight. The following day, the medium was replaced to remove the transfection complexes. Transient protein expression was assessed 24 to 48 h post-transfection, depending on the specific experimental requirements detailed in the figure legends. The same protocol was followed for siRNA-mediated knockdowns, except that Lipofectamine 2000 was used as the transfection reagent.

GFP trap for mass spectrometry experiment

For GFP-Trap, HeLa cells were transfected with TFEB-EGFP or EGFP in 140 mm dishes for 24–48 h. For harvesting, the cells were washed three times with ice-cold 1X PBS and collected in an ice-cold Eppendorf tube with 1 mL of 1X PBS. After centrifugation at 1000 rpm for 10 min at 4°C, the cell pellet was resuspended in 500–700 μL lysis buffer (10 mM Tris/Cl pH 7.5; 150 mM NaCl; 0.5 mM EDTA; 0.5% NP-40; containing protease and phosphatase inhibitors). After 30 min incubation on ice, the lysates were passed through a BD Micro-Fine+ 30G, 0.5mL insulin syringe every 10 min for a further 30 min. The insoluble fraction was removed by centrifugation of the lysate at 13000 rpm for 15 min. The supernatant was then collected in a pre-cooled tube and equilibrated

GFP-Trap_MA beads (pre-washed) were added, followed by end-over-end tumbling for 2 h at 4°C. After the incubation period, the beads were magnetically separated and washed three to four times with wash buffer (10 mM Tris/Cl pH 7.5; 150 mM NaCl; 0.5 mM EDTA). Finally, the beads were resuspended in 60 μL of 2X Laemmli buffer, vortexed and heated at 100°C for 10 min. The immunoprecipitation samples were then subjected to mass spectrometric analysis.

LC-MS/MS

Samples were resolved a short distance into a pre-cast minigel, the entire lane was excised and cut into 4 approximately equal sized chunks. The proteins were reduced, alkylated, and digested in-gel with the resulting tryptic peptides analyzed by LC-MS/MS using an OrbiTrap XL (Thermo Scientific) coupled to a nanoAcquity UHPLC (Waters). Raw files were converted to mzML using MSConvert (Proteowizard) and searched against a human Uniprot database (downloaded 090614, 20,264 entries) using MASCOT 2.3. Deamidation (N,Q) and oxidation (M) were set as variable modifications and carbamidomethylation (C) as a fixed modification. Peptide and protein identifications were validated in Scaffold 4.3.2. Peptide identifications greater than 90% probability, as established by Peptide Prophet, were accepted. Protein identification required greater than 95% probability and a minimum of 2 peptides.

Immunofluorescence

Cells for IF analysis were grown on coverslips and treated according to experimental requirements. Initial fixation was performed with 4% paraformaldehyde (PFA) in PBS for 10 min, followed by permeabilization with 0.1% Triton X-100 for 10 min, followed by blocking with 1% BSA in PBS for 20 min. The coverslips were then incubated with primary antibodies (diluted in 1% BSA) for 2 h, followed by a thorough wash with PBS. This was followed by incubation with Alexa Fluor-conjugated goat anti-mouse or rabbit secondary antibodies for 45 min in the dark at room temperature. After three PBS washes, samples were mounted with DAPI for nuclear staining. Imaging of IF samples was performed using an LSM880 confocal microscope (Zeiss), with subsequent analysis, quantification and processing using ImageJ software (NIH).

Proximity ligation assay (PLA)

HeLa cells overexpressing Myc-TFEB were used. To ensure specificity, antibodies from different species (mouse for Myc and rabbit for USP7) were used. Cells grown on coverslips were fixed with 4% paraformaldehyde for 5–7 min, followed by permeabilization with 0.1% Triton X-100 (v/v). The Duolink PLA fluorescence kit was used according to the manufacturer's instructions. Confocal microscopy imaging was performed the following day.

Immunoprecipitation

Co-immunoprecipitation experiments with Flag-TFEB used the same buffer conditions as GFP-Trap except for the use of Anti-Flag M2 magnetic beads.

For endogenous immunoprecipitation of USP7, the procedure mirrored that of GFP-Trap except that primary antibodies (e.g., anti-USP7 or IgG control) were added to clarified lysates for overnight incubation and end-over-end tumbling at 4°C. Subsequently, 50 μL of magnetic Dynabeads Protein A slurry was washed, added to the samples, and incubated for a further 2 h at 4°C. Finally, the beads were washed three times and proteins were eluted by boiling in Laemmli sample buffer.

A slightly modified lysis buffer (containing 10 mM Tris/Cl pH 7.5; 250 mM NaCl; 0.5 mM EDTA; 1% Triton X-100; supplemented with protease and phosphatase inhibitors and DUB inhibitor, PR-619) was used to assess the ubiquitination status of Flag-TFEB. After 2 h incubation, beads were magnetically separated. Beads were washed five times with the same lysis buffer instead of wash buffer.

Western blotting

Cellular protein levels were analyzed by western blotting. Cell lysis was performed using 1X Laemmli buffer, followed by loading of 20–30 μL of lysate onto a 10-well, 10–15% SDS-PAGE gel and electrophoresis at 100–120 V. A standard molecular weight ladder was co-loaded for gel monitoring. After electrophoresis, the proteins were transferred to activated PVDF membranes by semi-dry transfer. The membranes were then blocked with 5% skimmed milk or 1% BSA to prevent non-specific binding. Primary antibody incubation was performed overnight at 4°C, followed by washing with PBST. Secondary antibody incubation was performed for 1 h at room temperature. Secondary antibody dilutions were maintained at 1:5000 for ECL or 1:3000 for LICOR fluorophore-conjugated antibodies. After washing with PBST, the membranes were developed using ECL or imaged directly for fluorescence signal detection using LICOR Image Studio software.

Purification of ubiquitinated Flag-TFEB protein

To purify ubiquitinated Flag-TFEB protein, Anti-FLAG M2 magnetic beads conjugated to ubiquitinated Flag-TFEB were extracted from HEK293T cells. Five 140 mm dishes were precoated with poly-D-lysine prior to cell culture on day 1. On day 2, each dish was transfected with 20 μg of Flag-TFEB DNA in pen/strep-free medium. After a PBS wash on day 3, the medium was replaced with pen/strep-containing medium and the cells were left undisturbed for 48 h to maximise Flag-TFEB expression based on previous standardisation experiments. On purification day, cells were treated with MG132 (10 μM) and USP7 inhibitor (P22077- 5 μM) for 4 h and 30 min. Each plate was lysed using 1.3 mL of lysis buffer as described in the immunoprecipitation section and a similar protocol was followed with modifications to the washing steps. Magnetic beads were washed four times with high salt wash buffer (50 mM

HEPES pH 7.0–7.6, 200 mM NaCl, 5% glycerol, no detergent and no protease inhibitor, critical for downstream DUB reactions), followed by one wash with low salt buffer (50 mM HEPES pH 7.0–7.6, 50 mM NaCl, 5% glycerol). Flag beads were pooled, resuspended in low salt buffer and washed penultimately. The final wash of the Flag magnetic beads was performed with the *in vitro* deubiquitination reaction buffer, the composition of which is described in the following section.

In vitro DUB assay

An *in vitro* deubiquitination reaction was performed using Flag-TFEB immobilised on magnetic beads. Following a protocol adapted from Ji et al. (2019) for Axin, USP7 substrate, the beads were suspended in a deubiquitination reaction buffer containing 50 mM Tris-Cl pH 7.4, 150 mM NaCl, 5 mM MgCl2 and 5 mM dithiothreitol (DTT). Active recombinant USP7 enzyme, stored at −80°C, was thawed on ice. Experimental setups included three 40 μL reactions: one with only Flag-TFEB bound to magnetic beads at 37°C for 1 h (used as a control), another with Flag-TFEB and USP7 enzyme on ice (additional control), and the third with Flag-TFEB and USP7 enzyme at 37°C for 1 h. Reactions were gently mixed every 2 min for 1 h and then quenched with 13.5 μL of 4X sample buffer. Samples were subjected to western blot analysis. Duplicate samples were loaded on the gel to assess USP7 and Flag-TFEB/K48 separately.

Site-directed mutagenesis for point mutations

In this study, mass spectrometry was used to investigate the post-translational modifications of TFEB following USP7 inhibition. The results identified many potentially modified lysine residues, which were mutated to arginine using site-directed mutagenesis. The QuickChange Lightning Site-Directed Mutagenesis Kit from Agilent Technologies was used to generate K > R mutants of WT flag TFEB. Primers were designed using the. QuickChange primer design tool(https://www.agilent.com/store/primerDesignProgram.jsp), details of which are provided in Table S2. PCR reactions were performed according to the manufacturer's protocol using 50 ng of Flag TFEB dsDNA template. Due to the size of the plasmid (approximately 7 kb), an extension step of 4 min per cycle at 68°C was used. PCR products were subjected to Dpn I digestion at 37°C for 1 h before transformation into XL 10-Gold ultracompetent cells according to the manufacturer's instructions. Heat shock was followed by recovery in SOC media. By exploiting the ampicillin resistance marker of Flag-TFEB, the entire transformation reaction was plated on LB-ampicillin plates and positive mutants were identified by sequencing using the Sanger sequencing services of Source-BioScience.

Isolation of RNA and RT-PCR

RNA extraction was performed using the Qiagen RNeasy Kit, using a Trizol-free method based on column purification to obtain high quality RNA samples. Approximately 1 x 10^6 HeLa cells were subjected to relevant treatments, such as drug exposure or starvation, and RNA isolation was performed according to the manufacturer's protocol. Lysates were homogenised using the QIAshredder. RNAse-free tubes and pipette tips were used throughout to maintain RNA integrity. Finally, RNA samples were eluted in RNase-free water and stored at −80°C until further use for RT-PCR analysis using the Luna one-step RT-qPCR kit.

Flow cytometry

HeLa cells stably expressing SRAI-LC3B were harvested, washed with PBS, and detached from the plate using trypsin. The effect of trypsin was neutralised by serum containing media and cells were kept on ice throughout the process. Analysis was performed on an Attune NxT flow cytometer equipped with VL2 (405 512/25) and BL1 (488 530/30) detectors. To select cells expressing the SRAI-LC3B reporter protein, TOLLES-positive HeLa cells were identified by thresholding against unstained wild-type HeLa cells. Cells with greater VL2-A fluorescence than the distribution of unstained HeLa cells (TOLLES-CFPA+) were selected for further analysis using FlowJo software. To obtain a quantitative ratiometric readout, the mean TOLLES:YPet ratio of the TOLLES-CFP-A+ population was calculated as (VL2-A*100)/BL1-A using the 'Derive Parameters' function.

Lysotracker staining

HeLa cells were grown to 50–60% confluence in MatTek glass bottom culture dishes (P35G-1.0-14-C) on the day of treatment and imaging. The Lysotracker staining kit was used according to the manufacturer's instructions. Cells were treated with the appropriate concentration of Lysotracker reagent for 30 min. For the final 20 min of staining, Hoechst dye was added at a concentration of 1 μL per cell culture dish.

Prior to imaging, the cells were washed, and the staining medium was replaced with fresh medium. Live cell imaging was used to acquire microscopic images, and subsequent analysis was performed using ImageJ software.

Chromatin immunoprecipitation (ChIP) assay

HeLa TFEB knockout cells were transfected with either WT FLAG-TFEB or 3KR FLAG-TFEB. At 24 h post-transfection, cells were treated with Torin-1 for 1 h to ensure nuclear localisation of TFEB, regardless of the variant expressed. Cells were then fixed with formaldehyde to cross-link proteins to DNA, followed by lysis according to the manufacturer's instructions for the SimpleChIP Plus Enzymatic Chromatin IP Kit. Chromatin was partially digested with micrococcal nuclease to obtain optimal fragment sizes.

Chromatin immunoprecipitation was then performed using ChIP-validated anti-TFEB antibodies and ChIP-grade Protein G magnetic beads. After immunoprecipitation, the protein-DNA cross-links were reversed, and the DNA was purified using the DNA

purification spin columns provided in the kit. Enrichment of specific DNA sequences co-immunoprecipitated with TFEB was assessed by qPCR, focusing on promoters of CLEAR genes and including HPRT as a negative control. IgG rabbit antibody was used as a control for endogenous TFEB pull-down for ChIP experiments in HeLa WT cells to assess USP7 as a target gene, with the rest of the protocol being the same.

QUANTIFICATION AND STATISTICAL ANALYSIS

Data are presented as means ± standard error of the mean (SEM) from at least three independent experiments. The number of biological replicates (n) for each experiment, along with detailed statistical information, are provided in the respective figure legends. Statistical comparisons between two groups were performed using Student's t-test, while one-way or two-way ANOVA with appropriate post-hoc tests was used for comparisons involving more than two groups. All analyses were conducted using GraphPad Prism 10 (GraphPad Software, La Jolla, CA). A p-value of less than 0.05 was considered statistically significant.